Supplementary Information

Quantum engineering at the silicon surface using dangling bonds

Steven R. Schofield[1,2], Philipp Studer[1,3], Cyrus F. Hirjibehedin[1,2,4], Neil J. Curson[1,3], Gabriel Aeppli[1,2], & David R. Bowler[1,2]

[1]*London Centre for Nanotechnology, University College London, London, WC1H 0AH, UK*
[2]*Department of Physics and Astronomy, University College London, London, WC1E 6BT, UK*
[3]*Department of Electronic and Electrical Engineering, University College London, London, WC1E 7JE, UK*
[4]*Department of Chemistry, University College London, London, WC1H 0AJ, UK*

Supplementary Figures

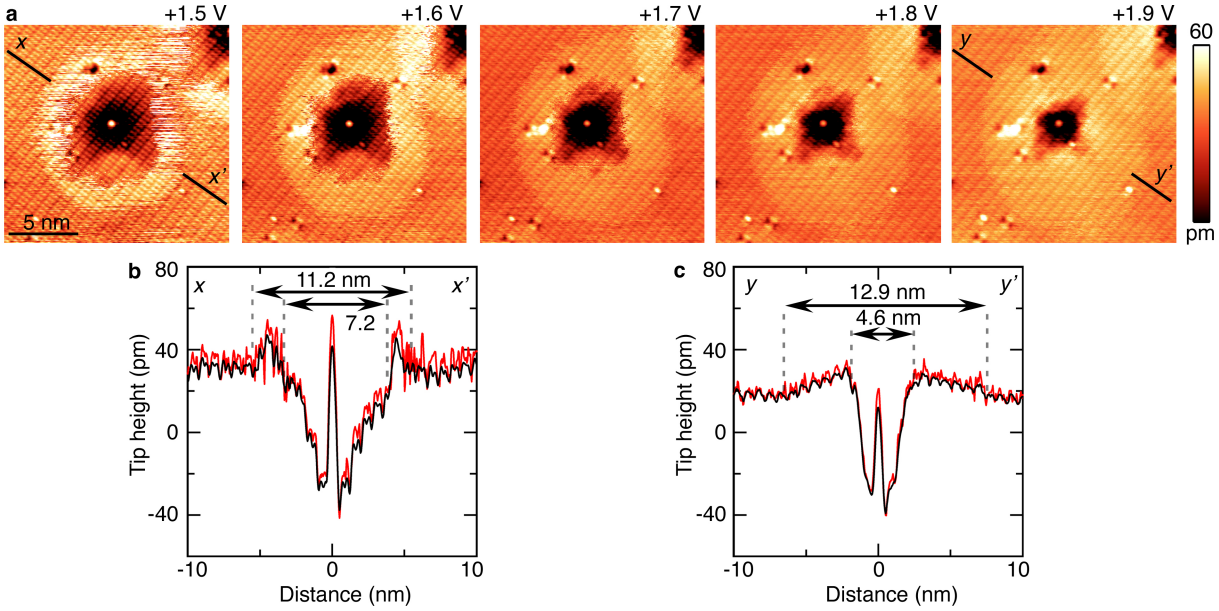

Supplementary Figure S1. Bias dependence of a single DB. a, STM topographic images of a single DB as a function of the tunnelling bias from $+1.5$ to $+1.9$ V with a constant tunnelling current set point of 25 pA. **b, c,** Line profiles taken across the $+1.5$ and $+1.9$ V images, as indicated in panel a. The red lines show a single profile across the centre of the DB, while the black lines show an average of 10 neighbouring profiles to to increase the signal to noise ratio.

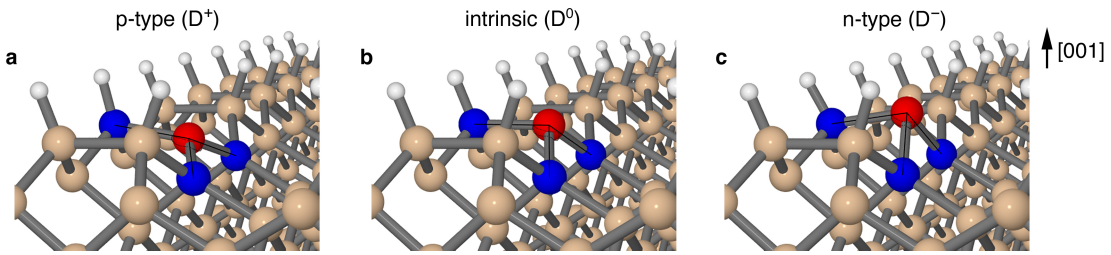

Supplementary Figure S2. DFT calculated structures for a single DB on Si(001):H. **a,** p-type, **b,** intrinsic, and **c,** n-type unit cells. Significant relaxation of the crystal occurs as the charge state of the DB changes from positive (D^+) to neutral (D^0) to negative (D^-). For clarity, the three-fold coordinated Si atom with the dangling bond is coloured red and the three atoms to which it is bonded are coloured blue. Hydrogen atoms are coloured white.

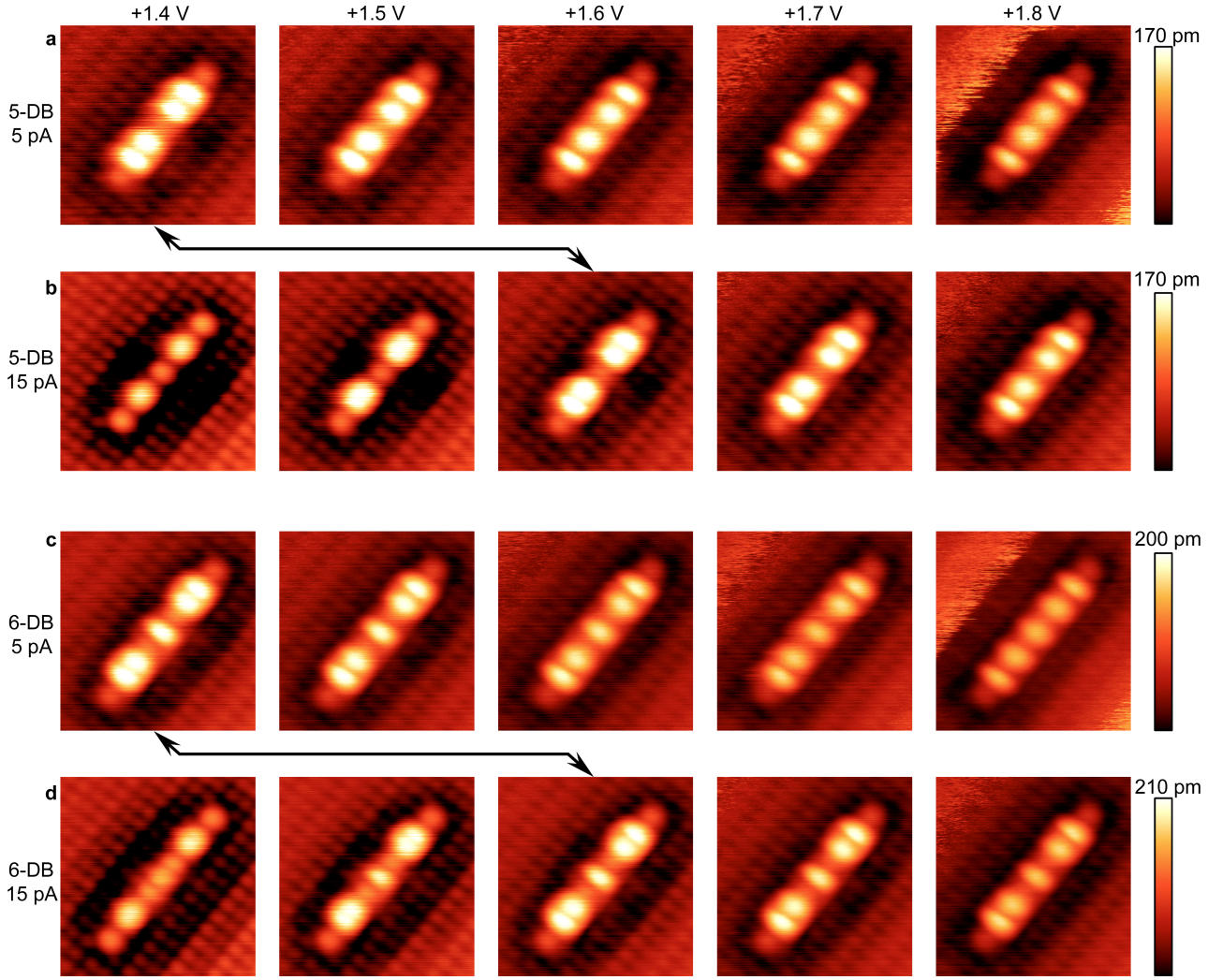

Supplementary Figure S3. Bias and current dependence of five- and six-DB chains. **a, b,** Five-DB chain imaged with $+1.4$ V to $+1.8$ V at 5 pA and 15 pA as indicated. **c, d,** Same image sequence for a six-DB chain. Double-headed arrows highlight examples of pairs of images that appear the same although they were acquired with different current-voltage settings; this demonstrates that the gating action of the tip on the surface can be altered by changing either the bias or the tunnelling current, and that for the images shown a 0.2 V bias change is equivalent to a 10 pA tunnelling current change.

Supplementary Tables

Supplementary Table S 1. DFT calculated energies for a single dangling bond (DB) on Si(001):H. DB energies are quoted in electronvolts with respect to the valence band maximum, and as a percentage of the calculated band gap E_{g}. Energies are quoted for two different k-points, Γ and K. The p-type DB is unoccupied, and the n-type DB is filled (2 electrons). For the intrinsic substrate, the DB level is spin-split into one filled and one empty single-electron level.

			Γ		K	
Unit cell	Defect state	Occupation	DB eV (%)	E_{g} eV	DB eV (%)	E_{g} eV
n-type	D^-	2	0.350 (45)	0.786	0.534 (46)	1.163
intrinsic	D^0	0	0.559 (68)	0.825	0.759 (63)	1.211
		1	0.013 (2)	0.825	0.119 (10)	1.211
p-type	D^+	0	0.011 (2)	0.744	0.236 (21)	1.154

Supplementary Note 1

Bias dependence of a single DB. Supplementary Figure S1a shows a series of STM topographic images of a single dangling bond acquired over a range of empty-state biases at constant tunnelling current. These images illustrate the bias dependence of the long-range Coulomb effects described in the main text. The diameter of the enhancement disc increases with bias: from 11.2 ± 0.8 nm at $+1.5$ V to 12.9 ± 0.8 nm at $+1.9$ V in Supplementary Figure S1a measured across the dimer rows as indicated. This is because the spatial extent of the electrostatic gating effect of the tip on the substrate scales with bias[25]. This has been described in detail in Ref. 26 where the ionisation of subsurface Si donors in a GaAs sample at 5 K were reported. Similar observations of STM tip induced ionisation have been reported for Co atoms on graphene [34] and C_{60} molecules on Al_2O_3/NiAl [35]. The spatial extent of the enhanced region depends also on the microscopic shape of the tip apex; this is because it is an effect of the electric field of the STM tip. The enhancement region only appears as a nearly circular "disc" as shown here in a subset of measurements in which the tip apex was very sharp and symmetrical. In other cases the enhancement region was observed to be elongated and/or asymmetric as expected when the STM tip apex is not symmetrical on the length scale relevant to the formation of the ionisation disc ($10 - 50$ nm)[26].

As described in the main text, the depression surrounding the DB in empty-state images indicates that the DB state is sufficiently decoupled from the substrate so that its charge state depends on the rates of charge transfer on and off the DB: the depression results when the rate of negative charge transfer from the STM tip to the DB level exceeds the rate of transfer from the DB to the substrate. This causes the DB to revert to the negatively charged D^- state, and the localised charge induces an upward shift in the surface energy bands that results in a decrease in the tunnelling current and the depression region in the image[16]. The phenomenon of non-equilibrium charging of a localised state between two tunnel barriers is well-known: it occurs in single-electron transistors (SET), and has been seen in STM-based experiments, e.g., where single metalorganic molecules were adsorbed on a thin (0.5 nm) insulating layer on top of a metal substrate[28], and for an isolated DB on the boron-saturated Si(111) surface[27]. There is a subtle distinction to be made in our case: the rate of charge transfer onto the DB level exceeds the rate of transfer off even when the tunnelling tip is still up to several nanometres away from the DB. This can perhaps be attributed to a large carrier capture cross-section: deep level transient spectroscopy (DLTS) measurements of P_{b} centre defects have shown they can have effective electron and hole

capture cross-sections of 10^{-14} cm^2 ($= 1$ nm^2) or more [36,37]. The presence of the surface and the influence of the tip may increase this further in the case of our measurements and we note that capture cross sections as large as 10^{-12} cm^2 ($= 100$ nm^2) have been reported for attractive Coulomb centres in silicon [38]. We gain further insight into the depression by observing its bias dependence: the spatial extent of the depression decreases with increasing empty-state bias (from 7.2 ± 0.8 nm to 4.6 ± 0.8 nm in Supplementary Figure S1a, measured perpendicular to the dimer row direction). This suggests that the relative rates of charging and discharging of the DB are shifting in favour of the discharging mechanism as the tip E_{F} is raised relative to the substrate bands. This is a natural consequence of the bias dependence of the tunnelling rate between the tip and sample. Both the transmission probability [39–44] and the tip local density of states (LDOS) [44–47] decrease rapidly for energies away from the tip E_{F} over an energy range of an electronvolt or so. Thus, the rate of electron tunnelling from the tip to the DB decreases rapidly as the empty-state bias is increased, resulting in a shrinking of the size of the depression region as observed.

The intention of this cursory discussion is to outline the salient points of the phenomenon, to provide additional credence to the tunnelling models presented in the main text and Figures 1 and 3, and to motivate further investigation and the development of an accurate quantitative model of this deceptively simple system.

Supplementary Note 2

DFT calculations of isolated DBs. We have calculated the properties of isolated DBs on the H-terminated Si(001) surface for intrinsic and charged unit cells; the calculation methodology is described in the *Supplementary Methods* section. The p- and n-type unit cells produced DB defect levels within the band gap at 11 meV and 350 meV above the valence band maximum (VBM) at the Γ point, respectively. These states were found to be essentially dispersionless, however, due to the curvature of the VBM they lie slightly higher above the VBM for k-points away from the Γ point, with the greatest difference being at the K-point (see Supplementary Table S1). In the case of the p-type unit cell, the DB was found to be entirely unoccupied and therefore positively charged (D^+), while for the n-type unit cell the DB was doubly-occupied and negatively charged (D^-). As might be expected by analogy with the clean Si(001) surface, there is significant lattice relaxation that accompanies the change in charge state of the DB, as shown in Supplementary Figure S2. The doubly-occupied negatively-charged D^- exhibits sp^3-like hybridisation, while the unoccupied, positively-charged D^+ has p-like character with sp^2-like bonds to the three neighbouring Si atoms. The calculation of the intrinsic unit cell produced an electrostatically-neutral state (D^0), with two nearly dispersionless single-electron *spin-split* levels, one occupied at 13 meV, and the other unoccupied at 559 meV above the VBM at the Γ point, in qualitative agreement with DFT calculations for a DB on the clean Si(001) surface[22].

Analogy with the $\mathrm{P_b}$ centre. There is a Coulomb energy cost, U, associated with localising two electrons (D^-) or two holes (D^+) onto the DB; this cost is offset to an extent by energy gains due to relaxation of the crystal lattice and local band structure changes, resulting in an effective charging energy, U^{eff} [48]. In electron paramagnetic resonance (EPR) this type of energy is known as the correlation energy, and gives the energy range over which the substrate E_{F} can be varied with the DB remaining electrostatically neutral, and hence exhibit non-zero spin. This energy can be estimated from our calculated defect energies using the equation[49], $U^{\mathrm{eff}} = D^- + D^+ - 2D^0$, which gives $U^{\mathrm{eff}} = 338$ meV using the Γ point values from Supplementary Table S1. This value is in good agreement with the measured correlation energy of dangling bonds that occur at the Si/SiO_2 interface—the so-called $\mathrm{P_b}$ centre defects. The $\mathrm{P_b}$ centre has different configurations, $\mathrm{P_{b0}}$ and $\mathrm{P_{b1}}$, which differ by their crystallographic orientation[50]. The $\mathrm{P_{b1}}$ centre is the most appropriate for comparison to (001) surface DBs, and its correlation energy was measured to be between $300-400$ meV using electron paramagnetic

resonance (EPR)[13], in good agreement with our figure of 338 meV. Furthermore, EPR measurements show that the P_{b1} levels lie in the lower half of the band gap[13]in agreement with DFT calculations of the P_{b1} centre[15], as well as our calculations of the Si(001) surface DB and our STM data. As an aside, we also note that the correlation energy of the P_{b0} centre—which has its axis parallel to the [111] direction—has been determined by EPR to be between 600 and 700 meV[13], and this is consistent with the figure of 750 meV recently determined using tunnelling spectroscopy measurements of a single DB on the Si(111) surface[27], further establishing the close correlation between surface DBs and their interfacial counterparts the P_b centres.

Supplementary Note 3

Bias and current dependence DB chains. Supplementary Figure S3 shows a series of STM images of 5- and 6-DB chains, acquired using different STM bias and current values. Each of the four panels a – d in this figure show a sequence of five images taken at sample biases of +1.4 to +1.8 V. Supplementary Figures S3a and S3b show a linear chain of five dangling bonds on next-nearest neighbour lattice sites taken at 5 and 15 pA, respectively. Supplementary Figures S3c and S3d show this same chain after the creation of one additional DB to create a 6-DB chain, and are also taken using 5 and 15 pA, respectively. Filled-state images of these five- and six-DB chains can be seen in Fig. 4 of the main text along with a description of the observed bound states. Of particular interest in Supplementary Figure S3 is the equivalence—in terms of the alignment between the tip and DB energy bands—of changing the tip bias or current set point. Arrows drawn between panels a and b, and panels c and d of Supplementary Figure S3 illustrate that changing the tunnel current by 10 pA has an effect on the band alignment equivalent to changing the bias by 0.2 V, as evident from the fact that the 1.4 V / 5 pA image appears the same as the 1.6 V / 15 pA image. By comparing the images taken at the higher voltages we see that the shift induced by the tunnel current change is linear with bias to within the accuracy of these measurements.

Supplementary Methods

Density functional theory calcluations. DFT calculations were performed using the VASP code[51,52] within the PW91 generalised gradient approximation (GGA)[53,54] using ultrasoft pseudopotentials[54]. The calculations used two dimer rows with eight dimers in each row, and between ten and eighteen layers of silicon with the bottom layer silicons terminated with two hydrogens and frozen in bulk-like positions. Electronic structure and energy differences were converged with a plane wave cutoff of 200 eV and Monkhurst-Pack k-mesh with $4\times1\times1$ k-points. The electronic structure was carefully converged with respect to slab thickness, and we found that eighteen layers of silicon were necessary to converge the band gap of the hydrogen terminated surface with respect to the bulk band gap. The cells ranged from 415 atoms to 671 atoms.

The calculations of charging of the dangling bonds were performed using two different methods: First, by doping the substrate with either Ga or P (for p-type or n-type doping); and second, by simply adjusting the occupancy by plus or minus one electron. Placing a net charge on a unit cell can cause convergence problems, particularly when vacuum is present in the unit cell. The second method (with a net charge) was tested carefully against the first, and no quantitative difference was found between the two, indicating that electrostatic effects were not significant in this case. The usual neutralising background approach to net charges was used in the calculation of electrostatic energy.

Supplementary References

34. Brar, V. W. *et al.* Gate-controlled ionization and screening of cobalt adatoms on a graphene surface. *Nature Phys.* **7**, 43–47 (2010).

35. Pradhan, N. A., Liu, N., Silien, C. & Ho, W. Atomic scale conductance induced by single impurity charging. *Phys. Rev. Lett.* **94**, 076801 (2005).
36. Johnson, N. M. Energy-resolved DLTS measurement of interface states in MIS structures. *Appl. Phys. Lett.* **34**, 802–804 (1979).
37. Johnson, N. M., Bartelink, D. J. & McVittie, J. P. Measurement of interface defect states at oxidized silicon surfaces by constantcapacitance DLTS. *J. Vac. Sci. Technol.* **16**, 1407–1411 (1979).
38. Lax, M. Cascade capture of electrons in solids. *Phys. Rev.* **119**, 1502–1523 (1960).
39. Hamers, R. J. Methods of tunneling spectroscopy with STM. In Bonnell, D. A. (ed.) *Scanning probe microscopy and spectroscopy: theory, techniques and applications* (Wiley-VCH, 2001).
40. Grobis, M., Wachowiak, A., Yamachika, R. & Crommie, M. F. Tuning negative differential resistance in a molecular film. *Appl. Phys. Lett.* **86**, 204102 (2005).
41. Tu, X. W., Mikaelian, G. & Ho, W. Controlling Single-Molecule Negative Differential Resistance in a Double-Barrier Tunnel Junction. *Phys. Rev. Lett.* **100**, 126807 (2008).
42. Lyo, I.-W. & Avouris, P. Negative differential resistance on the atomic scale: implications for atomic scale devices. *Science* **245**, 1369–1371 (1989).
43. Avouris, P., Lyo, I.-W., Bozso, F. & Kaxiras, E. Adsorption of boron on Si (111): Physics, chemistry, and atomic-scale electronic devices. *J. Vac. Sci. Tech. A* **8**, 3405–3411 (1990).
44. Xue, Y. *et al.* Negative differential resistance in the scanning-tunneling spectroscopy of organic molecules. *Phys. Rev. B* **59**, R7852–R7855 (1999).
45. Lang, N. & Williams, A. Theory of atomic chemisorption on simple metals. *Phys. Rev. B* **18**, 616–636 (1978).
46. Yeyati, A. L., Martín-Rodero, A. & Flores, F. Conductance quantization and electron resonances in sharp tips and atomic-size contacts. *Phys. Rev. B* **56**, 10369–10372 (1997).
47. Agraït, N., Yeyati, A. L. & van Ruitenbeek, J. M. Quantum properties of atomic-sized conductors. *Phys. Rep.* **377**, 81–279 (2003).
48. Anderson, P. W. Model for the electronic structure of amorphous semiconductors. *Phys. Rev. Lett.* **34**, 953–955 (1975).
49. Northrup, J. Effective correlation energy of a Si dangling bond calculated with the local-spin-density approximation. *Phys. Rev. B* **40**, 5875–5878 (1989).
50. Kato, K., Yamasaki, T. & Uda, T. Origin of P_{b1} center at $SiO_2Si(100)$ interface: first-principles calculations. *Phys. Rev. B* **73**, 073302 (2006).
51. Kresse, G. & Furthmüller, J. Efficient iterative schemes for ab initio total-energy calculations using a plane-wave basis set. *Phys. Rev. B* **54**, 11169–11186 (1996).
52. Kresse, G. Ab initio molecular dynamics for liquid metals. *Phys. Rev. B* **47**, 558–561 (1993).
53. Vanderbilt, D. Soft self-consistent pseudopotentials in a generalized eigenvalue formalism. *Phys. Rev. B* **41**, 7892–7895 (1990).
54. Perdew, J. P. & Wang, Y. Accurate and simple analytic representation of the electron-gas correlation energy. *Phys. Rev. B* **45**, 13244–13249 (1992).